Available online at www.sciencedirect.com
SCIENCE DIRECT®
Journal of Sound and Vibration 290 (2006) 223–241
JOURNAL OF SOUND AND VIBRATION
www.elsevier.com/locate/jsvi

Modal analysis and shape optimization of rotating cantilever beams

Hong Hee Yoo[a,*], Jung Eun Cho[b], Jintai Chung[c]

[a]*School of Mechanical Engineering, Hanyang University, 17 Haengdang-Dong Sungdong-Gu, Seoul 133-791, Republic of Korea*
[b]*R&D Center Chassis Team, Hyundai Motor Company, Jangduk-Dong, Whasung-Si, Kyunggi-Do 445-706, Republic of Korea*
[c]*Department of Mechanical Engineering, Hanyang University, 1271 Sa-1-Dong, Ansan, Kyunggi-Do 425-791, Republic of Korea*

Received 12 February 2004; received in revised form 9 March 2005; accepted 26 March 2005
Available online 21 June 2005

Abstract

When a cantilever beam rotates about an axis perpendicular to its neutral axis, its modal characteristics often vary significantly. If the geometric shape and the material property of the beam are given, the modal characteristic variations can be accurately estimated following a well-established analysis procedure employing assumed mode method or finite element method. In many practical design situations, however, some modal characteristics are usually specified as design requirements and the geometric shape that satisfies the requirements needs to be found. In the present study, certain modal characteristic requirements such as maximum or minimum slope natural frequency loci are specified and the geometric shapes that satisfy the requirements are obtained through an optimization procedure.

*Corresponding author. Tel.: +82 2 2290 0446; fax: +82 2 2293 0570.
E-mail addresses: hhyoo@hanyang.ac.kr (H.H. Yoo), jecho@hyundai-motor.com (J.E. Cho), jchung@hanyang.ac.kr (J. Chung).

0022-460X/$ - see front matter © 2005 Elsevier Ltd. All rights reserved.
doi:10.1016/j.jsv.2005.03.014

1. Introduction

Cantilever beam-like structures can be found in many practical engineering examples. To design such structures, it is necessary to calculate natural frequencies to avoid undesirable problems such as resonance phenomena. It is a common practice to find the natural frequencies of stationary structures if their geometric and material properties are given. Some cantilever structures (for instance, turbine and helicopter blades), however, rotate during their normal operation. Due to the rotational motion, the modal characteristics of cantilever structures often vary significantly. Therefore, the variations of modal characteristics need to be estimated accurately for reliable designs of the rotating structures.

Southwell and Gough [1] pioneered to investigate the modal characteristics of rotating cantilever beams in 1920s, and their monumental work was followed by many theoretical and numerical studies (see, for instance, Refs. [2–5]). More recently, advanced methods were developed and more complicated effects (see, for instance, Refs. [6–12]) were considered to analyze the modal characteristics of rotating structures. Using these methods, the modal characteristics of rotating cantilever structures could be effectively analyzed if the geometric and the material properties are given. However, in many practical design situations, the geometric shapes of rotating structures need to be found (instead of being given) while their modal characteristics are specified as design requirements (to avoid undesirable vibration problems). Despite the best effort of the authors, research works on such inverse problems were rarely found in literature.

The purpose of the present study is to find the optimal shapes of rotating cantilever beams that provide some specific modal characteristics. Maximal or minimal increasing rate of a natural frequency versus the angular speed could be one of the specific modal characteristics. In the present study, the cross-section of the rotating beam is assumed rectangular and the length of the beam is divided into multiple segments. The thickness and the width at every segment are assumed to be cubic spline functions. The stage (the segment's ends) values of the thickness and the width are employed as design variables and optimization problems that include the design requirements of specific modal characteristics are formulated. An optimization method that combines a genetic algorithm [13] along with a gradient-based search algorithm [14] is employed to solve the problems in the present study.

2. Derivation of the modal equations of a rotating cantilever beam

In the present study, a linear dynamic modeling method that employs hybrid deformation variables (see Ref. [11]) is utilized to derive the equations of motion for rotating cantilever beams. The following assumptions are employed. Firstly, the beam has homogeneous and isotropic material properties. Secondly, the beam has slender shape so that shear and rotary inertia effects are ignored. Finally, the stretching and the out-of-plane bending deformations are only considered. These assumptions are made to simplify the modeling procedure and to focus on the major interest of the present study, that is how to find the optimal shape of rotating beams that satisfy certain design requirements of modal characteristics.

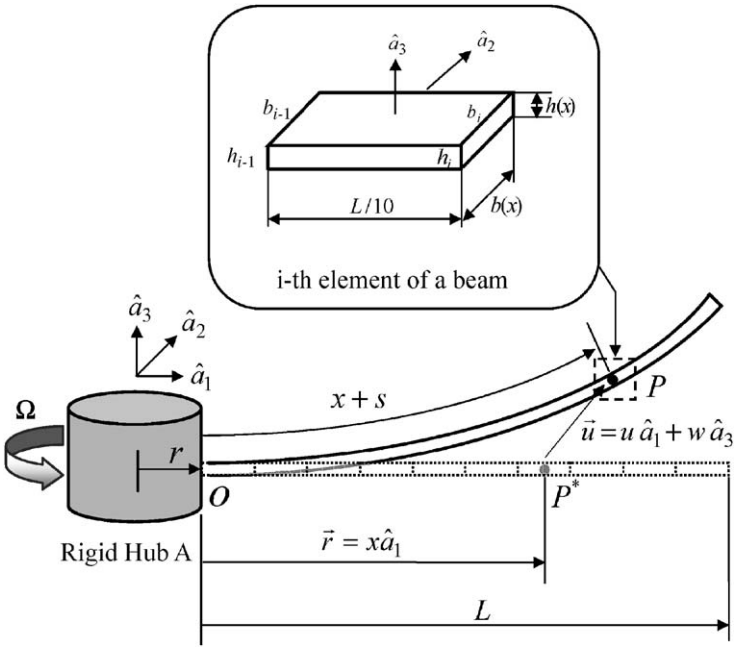

Fig. 1. Configuration of a rotating cantilever beam.

Fig. 1 shows the configuration of a cantilever beam fixed to a rigid hub (reference frame A) that rotates with constant angular speed Ω about the axis of $\hat{a}_3$. In the figure, $\hat{a}_1$, $\hat{a}_2$, and $\hat{a}_3$ represent orthogonal unit vectors fixed in the rigid hub; $\vec{u}$ denotes the elastic deformation of a generic point; u and w denote the axial and the out-of-plane bending deformation components, respectively; and s denotes the arc-length stretch (stretch along the deformed beam axis). The angular velocity of the rigid hub A and the velocity of point O can be expressed as follows:

$$\vec{\omega}^A = \Omega\hat{a}_3, \quad \vec{v}^O = r\Omega\hat{a}_2, \tag{1}$$

where r denotes the radius of the rigid hub. Then the velocity of the generic point P can be derived as follows:

$$\vec{v}^P = [\dot{u}]\hat{a}_1 + [\Omega(r+x+u)]\hat{a}_2 + [\dot{w}]\hat{a}_3, \tag{2}$$

where x is the distance from point O to the generic point in the un-deformed configuration.

In the present work, s and w are approximated (by employing the assumed mode method) as follows:

$$s(x,t) = \sum_{j=1}^{\mu_1} \phi_{1j}(x)q_{1j}(t),$$

$$w(x,t) = \sum_{j=1}^{\mu_2} \phi_{2j}(x)q_{2j}(t), \tag{3}$$

where ϕ_{1j} and ϕ_{2j} are mode functions, q_{1j} and q_{2j} are generalized coordinates and μ_1 and μ_2 are the numbers of the generalized coordinates. Since the non-Cartesian variable s is approximated, the following geometric relation needs to be employed to derive the equations of motion.

$$x + s = \int_0^x \left[\left(1 + \frac{\partial u}{\partial \sigma} \right)^2 + \left(\frac{\partial w}{\partial \sigma} \right)^2 \right]^{1/2} \mathrm{d}\sigma. \tag{4}$$

Using a binomial expansion of Eq. (4)

$$s = u + \frac{1}{2} \int_0^x \left(\frac{\partial w}{\partial \sigma} \right)^2 \mathrm{d}\sigma + (\text{higher degree terms}). \tag{5}$$

Differentiation of the above equation with respect to time gives

$$\dot{s} = \dot{u} + \int_0^x \left(\frac{\partial w}{\partial \sigma} \right) \left(\frac{\partial \dot{w}}{\partial \sigma} \right) \mathrm{d}\sigma + (\text{higher degree terms}). \tag{6}$$

By substituting Eqs. (5) and (6) (while neglecting the higher degree terms) into Eq. (2), the velocity of the generic point P can be obtained as follows:

$$\vec{v}^P = \left[\dot{s} - \int_0^x \left(\frac{\partial w}{\partial \sigma} \right) \left(\frac{\partial \dot{w}}{\partial \sigma} \right) \mathrm{d}\sigma \right] \hat{a}_1 + \left[\Omega \left(r + x + s - \frac{1}{2} \int_0^x \left(\frac{\partial w}{\partial \sigma} \right)^2 \mathrm{d}\sigma \right) \right] \hat{a}_2 + [\dot{w}] \hat{a}_3. \tag{7}$$

The partial derivatives of the velocity of P with respect to the generalized speeds ($\dot{q}_{1i}$ and $\dot{q}_{2i}$) can be obtained as follows:

$$\begin{aligned} \frac{\partial \vec{v}^P}{\partial \dot{q}_{1i}} &= \phi_{1i} \hat{a}_1 && (i = 1, 2, \ldots, \mu_1), \\ \frac{\partial \vec{v}^P}{\partial \dot{q}_{2i}} &= -\left[\sum_{j=1}^{\mu_2} \left(\int_0^x \phi_{2i,\sigma} \phi_{2j,\sigma} \, \mathrm{d}\sigma \right) q_{2j} \right] \hat{a}_1 + \phi_{2i} \hat{a}_3 && (i = 1, 2, \ldots, \mu_2). \end{aligned} \tag{8}$$

Later, Eq. (8) will be employed to obtain the generalized inertia forces in the equations of motion.

Now, to obtain the generalized active forces in the equations of motion, one needs the strain energy expression of the beam, which is expressed as follows:

$$U = \frac{1}{2} \int_0^L \left[EA^* \left(\frac{\partial s}{\partial x} \right)^2 + EI_{yy} \left(\frac{\partial^2 w}{\partial x^2} \right)^2 \right] \mathrm{d}x, \tag{9}$$

where L denotes the beam length, E denotes Young's modulus, A^* denotes the cross-sectional area and I_{yy} denotes the second area moment of the cross-section. With the assumption of neglecting rotary inertia effect, the equations of motion can be obtained from the following equation:

$$\int_0^L \rho A^* \left(\frac{\partial \vec{v}^P}{\partial \dot{q}_i} \right) \cdot \vec{a}^P \, \mathrm{d}x + \frac{\partial U}{\partial q_i} = 0 \quad (i = 1, 2, \ldots, \mu), \tag{10}$$

where ρ denotes the density, q_i consists of q_{1i} and q_{2i}, μ is the sum of μ_1 and μ_2 and $\vec{a}^P$ denotes the acceleration of the generic point which can be obtained by differentiating the velocity expression given in Eq. (7). Employing Eq. (10), the equations of motion can be finally derived

as follows:

$$\sum_{j=1}^{\mu_1}\left(\int_0^L \rho A^*\phi_{1i}\phi_{1j}\,\mathrm{d}x\right)\ddot{q}_{1j}-\sum_{j=1}^{\mu_1}\left[\Omega^2\left(\int_0^L \rho A^*\phi_{1i}\phi_{1j}\,\mathrm{d}x\right)-\left(\int_0^L EA^*\phi_{1i,x}\phi_{1j,x}\,\mathrm{d}x\right)\right]q_{1j}$$
$$-r\Omega^2\left(\int_0^L \rho A^*\phi_{1i}\,\mathrm{d}x\right)-\Omega^2\left(\int_0^L \rho A^*x\phi_{1i}\,\mathrm{d}x\right)$$
$$=0\quad(i=1,2,\ldots,\mu_1), \tag{11}$$

$$\sum_{j=1}^{\mu_2}\left(\int_0^L \rho A^*\phi_{2i}\phi_{2j}\,\mathrm{d}x\right)\ddot{q}_{2j}+\sum_{j=1}^{\mu_2}\left(\int_0^L EI_{yy}\phi_{2i,xx}\phi_{2j,xx}\,\mathrm{d}x\right)q_{2j}$$
$$+\sum_{j=1}^{\mu_2}\Omega^2\left[\int_0^L \rho A^*x\left(\int_0^x \phi_{2i,\sigma}\phi_{2j,\sigma}\,\mathrm{d}\sigma\right)\mathrm{d}x\right]q_{2j}+\sum_{j=1}^{\mu_2}r\Omega^2\left[\int_0^L \rho A^*\left(\int_0^x \phi_{2i,\sigma}\phi_{2j,\sigma}\,\mathrm{d}\sigma\right)\mathrm{d}x\right]q_{2j}$$
$$=0\quad(i=1,2,\ldots,\mu_2). \tag{12}$$

As can be observed from Eqs. (11) and (12), the bending equations are decoupled from the stretching equations. Since natural frequencies of bending modes are much lower than those of stretching modes, only the bending equations will be employed for the modal analysis. Using matrix notation, the bending equations can be expressed as follows:

$$[M]\{\ddot{q}_2\}+\langle[K^B]+\Omega^2[K^G]\rangle\{q_2\}=0, \tag{13}$$

where the elements of $[M]$, $[K^B]$, and $[K^G]$ are defined as follows:

$$M_{ij}\equiv\int_0^L \rho bh\phi_{2i}\phi_{2j}\,\mathrm{d}x, \tag{14}$$

$$K^B_{ij}\equiv\int_0^L E\frac{bh^3}{12}\phi_{2i,xx}\phi_{2j,xx}\,\mathrm{d}x, \tag{15}$$

$$K^G_{ij}\equiv\int_0^L \rho bh(x+r)\left(\int_0^x \phi_{2i,\sigma}\phi_{2j,\sigma}\,\mathrm{d}\sigma\right)\mathrm{d}x, \tag{16}$$

where b and h denote the width and the thickness of the rectangular cross-section, respectively. The length of the beam is equally divided into n segments and the thickness and the width at every segment are assumed as cubic spline functions, which can be expressed, respectively, as follows:

$$f_i(x)=a_i^t\left(x-\frac{(i-1)\times L}{n}\right)^3+b_i^t\left(x-\frac{(i-1)\times L}{n}\right)^2+c_i^t\left(x-\frac{(i-1)\times L}{n}\right)+d_i^t,$$
$$g_i(x)=a_i^w\left(x-\frac{(i-1)\times L}{n}\right)^3+b_i^w\left(x-\frac{(i-1)\times L}{n}\right)^2$$
$$+c_i^w\left(x-\frac{(i-1)\times L}{n}\right)+d_i^w\quad(i=1,\ldots,n). \tag{17}$$

All the coefficients of the cubic spline functions (for the thickness and the width) can be determined by the following conditions:

$$f_i\left(\frac{i\times L}{n}\right)=h_i,\quad g_i\left(\frac{i\times L}{n}\right)=b_i\quad (i=1,\ldots,n), \tag{18}$$

$$f_i\left(\frac{i\times L}{n}\right)=f_{i+1}\left(\frac{i\times L}{n}\right),\quad g_i\left(\frac{i\times L}{n}\right)=g_{i+1}\left(\frac{i\times L}{n}\right),$$

$$f_i'\left(\frac{i\times L}{n}\right)=f_{i+1}'\left(\frac{i\times L}{n}\right),\quad g_i'\left(\frac{i\times L}{n}\right)=g_{i+1}'\left(\frac{i\times L}{n}\right)\quad (i=1,\ldots,n-1),$$

$$f_i''\left(\frac{i\times L}{n}\right)=f_{i+1}''\left(\frac{i\times L}{n}\right),\quad g_i''\left(\frac{i\times L}{n}\right)=g_{i+1}''\left(\frac{i\times L}{n}\right), \tag{19}$$

$$f_1(0)=h_0,\quad g_1(0)=b_0,$$

$$f_1''(0)=f_n''(L)=0,\quad g_1''(0)=g_n''(L)=0. \tag{20}$$

By using the local spline functions, the global thickness function $h(x)$ and the global width function $b(x)$ can be expressed as follows:

$$h(x)=\sum_{i=1}^{n} f_i(x)u_i(x),$$

$$b(x)=\sum_{i=1}^{n} g_i(x)u_i(x), \tag{21}$$

where

$$\text{if } x=0\quad \text{then } u_1(0)=1 \text{ and } u_i(0)=0\quad (i\neq 1),$$

$$\text{if } x\in\left(\frac{(k-1)\times L}{n},\frac{k\times L}{n}\right]\quad \text{then } u_k(x)=1 \text{ and } u_i(x)=0\quad (i\neq k).$$

Now by using the global thickness and width functions in Eq. (21), the elements of the mass and the stiffness matrices shown in Eqs. (14)–(16) can be calculated and the modal analysis employing Eq. (13) can be performed.

To verify the accuracy of the modal formulation (that is derived in this section), three test problems are solved. Fig. 2 shows the shapes of the three cantilever beams and the corresponding shape functions. The material and geometric data are given in Table 1. Numerical results obtained

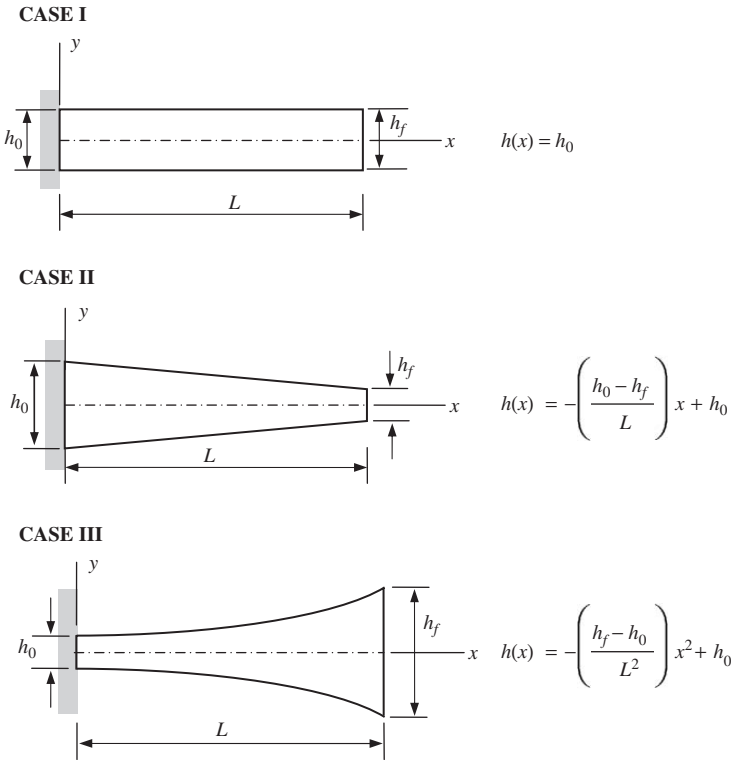

Fig. 2. Beam thickness variations of three cases of test problems.

Table 1
Comparison of the first natural frequency

Angular velocity	Case I		Case II		Case III	
	Present	ANSYS	Present	ANSYS	Present	ANSYS
0	2.3409	2.3405	2.6814	2.6812	0.58161	0.58124
10	2.9132	2.9128	3.2408	3.2407	1.7707	1.7698
20	4.1649	4.1651	4.4847	4.4852	3.3515	3.3457
30	5.6349	5.6371	5.9540	5.9562	4.9526	4.9374

(*unit*: rad/s).

by the present method and a commercial code ANSYS are compared in Table 2. To obtain the present results, the beam is divided into 10 segments in which the thickness is expressed with a spline function. To obtain the results of ANSYS, the beam is divided into 50 segments in which the thickness is expressed with a linear function. Table 2 shows that the numerical results obtained by the two methods are in good agreement.

Table 2
Material and geometric properties of the beam for test problems

Description	Case I	Case II	Case III
Young's modulus (E) (GPa)	70		
Density (ρ) (kg/m^3)	1.2×10^3		
Length (L) (m)	10		
Width (b) (m)	0.3		
Fixed end height (h_0) (m)	0.3	0.3	0.1
Free end height (h_f) (m)	0.3	0.1	0.3

Table 3
Material and geometric properties of the beam for optimization problems

Description	Data
Young's modulus (E) (GPa)	69.0
Density (ρ) (kg/m^3)	2.71×10^3
Length (L) (m)	0.4

3. Formulation of optimization problems and numerical results

The natural frequencies of rotating beams can be determined from the angular speed as well as the thickness and the width that consist of the cross-section. Thus, the natural frequencies can be expressed as follows:

$$\omega_k = \omega_k(\Omega, X), \tag{22}$$

where ω_k denotes the kth natural frequency, Ω denotes the angular speed of the rotating beam, and X denotes the stage values of the thickness and the width, which are employed as design variables. Thus, if a beam is divided into n segments, X can be expressed as follows:

$$X = [h_0, h_1, \ldots, h_n, b_0, b_1, \ldots, b_n]^{\mathrm{T}}, \tag{23}$$

where h_i and b_i represent the stage values of the thickness and the width from the fixed end to the free end of the cantilever beam, respectively. The material and geometric properties of the beam are given in Table 3. To obtain the natural frequencies, five bending modes are employed.

3.1. Problem to find the range of the first natural frequency of a rotating beam

The first problem is to find the range of the first natural frequency of a rotating beam when the following constraints are given. The total volume of the beam needs to be not larger than the initial volume and the thickness and the width have minimum values. To solve the problem,

the objective function and the constraints are formulated as follows:

$$\begin{aligned} \text{Min (or Max)} \quad & \omega_1(\Omega_s, X) \\ \text{s.t.} \quad & \int_0^L h(X,x)b(X,x)\,\mathrm{d}x \leqslant Lh_{\text{ini}}b_{\text{ini}}, \\ & h(X,x) \geqslant h_{\min} \quad (0 \leqslant x \leqslant L), \\ & b(X,x) \geqslant b_{\min} \quad (0 \leqslant x \leqslant L), \end{aligned} \tag{24}$$

where Ω_s denotes the angular speed; $h_{\text{ini}}(= 0.002\,\text{m}$ and $b_{\text{ini}}(= 0.035\,\text{m})$ denote the initial thickness and the initial width; and $h_{\min}(= 0.001\,\text{m})$ and $b_{\min}(= 0.0175\,\text{m})$ denote the minimum thickness and the minimum width of the cross-section. For this problem, the hub radius is given 0 and the length of the beam is divided into 10 segments. Thus, the design variables consist of 22 elements.

Fig. 3 shows the minimum and the maximum first natural frequency loci of the rotating beam when the angular speed increases from 0 to 300 rad/s. Therefore, the two loci embrace the possible region of the first natural frequency of the rotating beam. To obtain the results in Fig. 3, two optimization problems (to find the minimum and the maximum natural frequencies) for the angular speed of 0 rad/s, are first solved with the given initial design variables. The optimum values of design variables are then employed as the initial values to solve the optimization problems for the angular speed of 0.1 rad/s. The same procedure continues until the angular speed reaches 300 rad/s. Thus, 3001 sets of optimization problems need to be solved to obtain the minimum and the maximum loci, respectively. Table 4 shows a typical set of numerical results for the optimization problem. The initial and the optimal values of the design variables and the objective function (to find the first minimum natural frequency) for the angular speed of 0 rad/s are shown in the table. Fig. 4 also shows the convergence history of the objective function.

Figs. 5 and 6 represent the thickness and the width of the beam versus the length of the beam for the minimum and the maximum first natural frequency results, respectively. The thickness and the width variations along the beam length for the angular speed of 0 and 300 rad/s are shown in

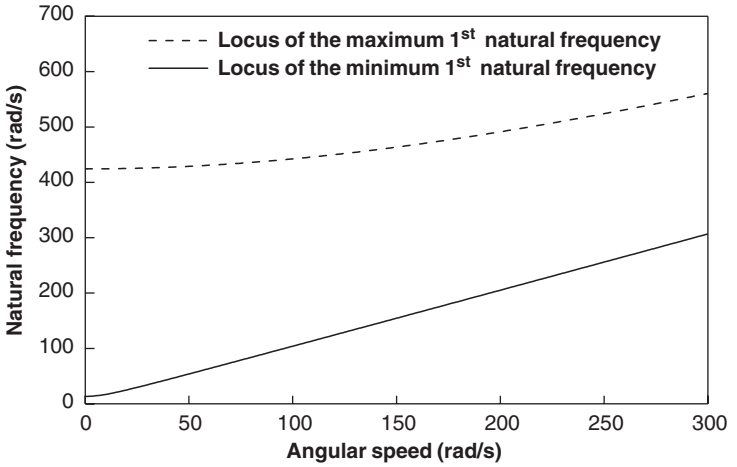

Fig. 3. Two loci that embrace the first natural frequency range.

Table 4
Initial and optimal values of the design variables and the objective function

	Initial values	Optimal values
Design variables (m)		
h_0	0.002	0.00100
h_1	0.002	0.00100
h_2	0.002	0.00102
h_3	0.002	0.00114
h_4	0.002	0.00144
h_5	0.002	0.00195
h_6	0.002	0.00275
h_7	0.002	0.00389
h_8	0.002	0.00542
h_9	0.002	0.00740
h_{10}	0.002	0.00989
b_0	0.035	0.01750
b_1	0.035	0.01811
b_2	0.035	0.01873
b_3	0.035	0.01938
b_4	0.035	0.02006
b_5	0.035	0.02076
b_6	0.035	0.02148
b_7	0.035	0.02223
b_8	0.035	0.02301
b_9	0.035	0.02382
b_{10}	0.035	0.02465
Objective function (rad/s)	64.019	13.190

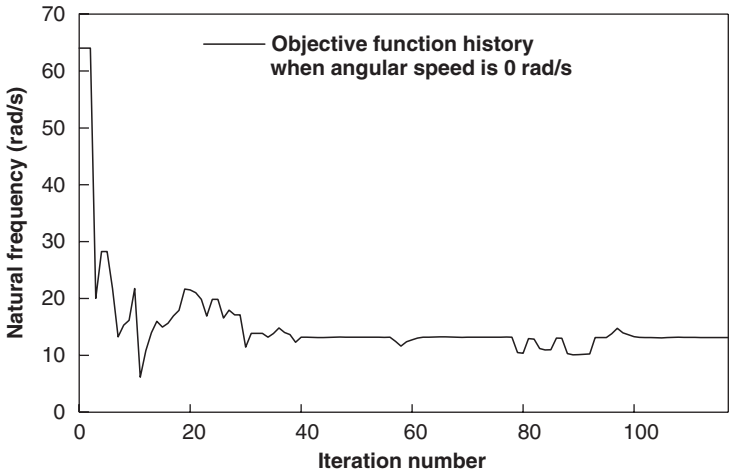

Fig. 4. Convergence history of the objective function.

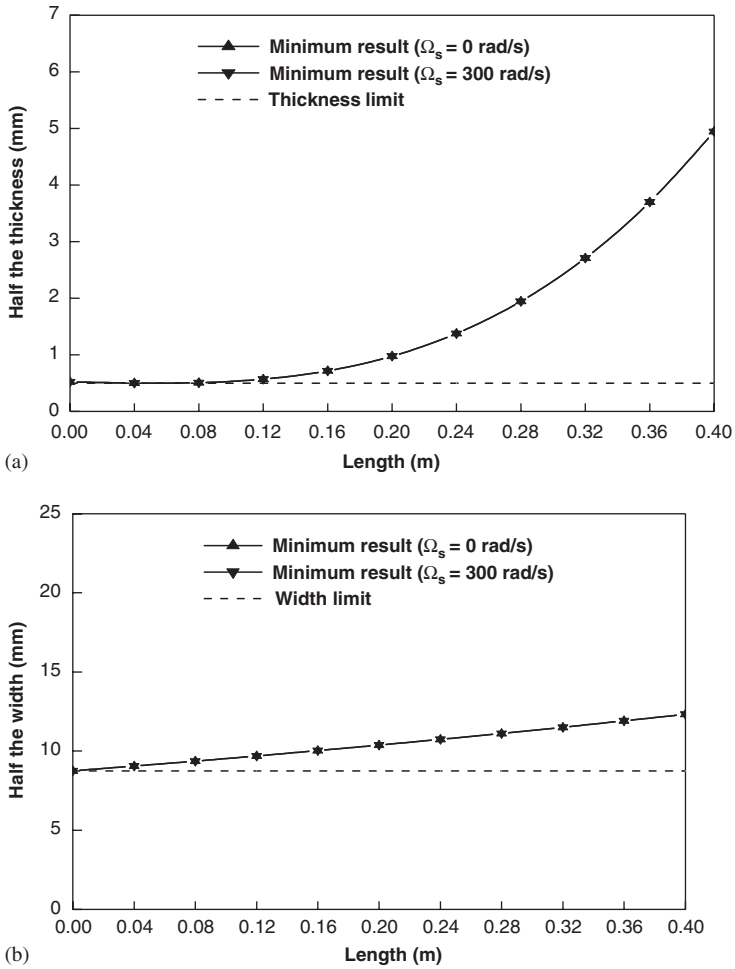

Fig. 5. Variation of the thickness and the width along the beam length that minimize the first natural frequency. (a) Half the thickness, (b) half the width.

these figures. The minimum frequency results show that both the thickness and the width gradually increase as the cross-section moves to the free end. The maximum frequency results, however, show that the width fixes to the minimum value, $b_{\min}$ while the thickness varies with an interesting curve. The thickness curve has three peaks that decrease as the cross-section moves to the free end. These figures also show that the cross-section shapes that minimize and maximize the first natural frequencies do not vary even if the angular speed varies. Figs. 7 and 8 show the overall pictures of the beams for the minimum and the maximum frequency results, respectively. To show cross-sections of the beams in detail, the thickness and the width are amplified two times compared to the length of the beam.

It is well known that (as the angular speed increases) the natural frequencies of cantilever beams with larger hub radius increase faster than those with smaller hub radius. To investigate the effect of the hub radius on the optimal shape of rotating beam, problems with different hub radius

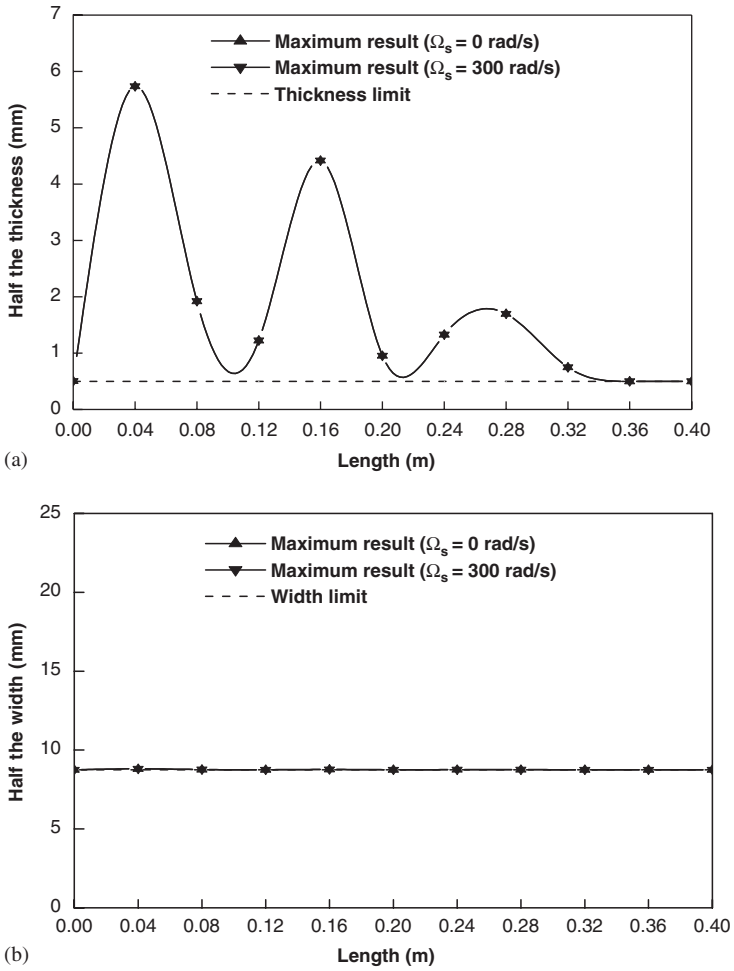

Fig. 6. Variation of the thickness and the width along the beam length that maximize the first natural frequency. (a) Half the thickness, (b) half the width.

values are solved. Fig. 9 shows the thickness and the width of the beam (that maximize the first natural frequency) with three different radius values. The results show that the optimal shapes for the three different radius values are identical. So, for other design problems, hereinafter, the hub radius of the rotating beam is fixed as 0.

3.2. *Problem with the fixed stationary first natural frequency constraint*

In many structural design problems, the stationary first natural frequency (when the angular speed is zero) often needs to be constrained to the initially given value. So one more constraint (as a design requirement) is added to the previous problem. Thus, the objective function and

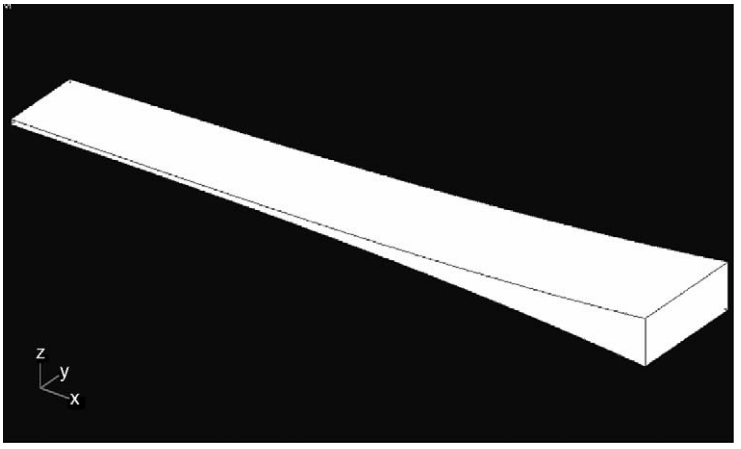

Fig. 7. Beam shape that minimizes the first natural frequency.

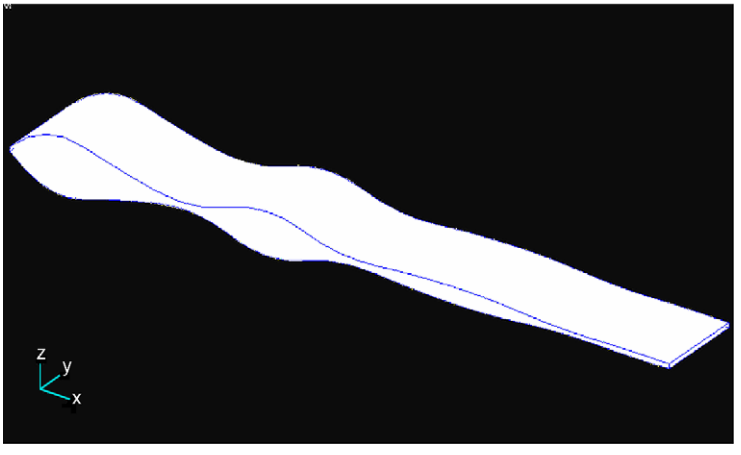

Fig. 8. Beam shape that maximizes the first natural frequency.

constraints are now given as follows:

$$\begin{aligned} \text{Min (or Max)} \quad & \omega_1(\Omega_s, X) \\ \text{s.t.} \quad & \omega_1(0, X) - \omega_1(0, X_0) = 0, \\ & \int_0^L h(X,x)b(X,x)\,\mathrm{d}x \leqslant Lh_{\text{ini}}b_{\text{ini}}, \\ & h(X,x) \geqslant h_{\min} \quad (0 \leqslant x \leqslant L), \\ & b(X,x) \geqslant b_{\min} \quad (0 \leqslant x \leqslant L). \end{aligned} \tag{25}$$

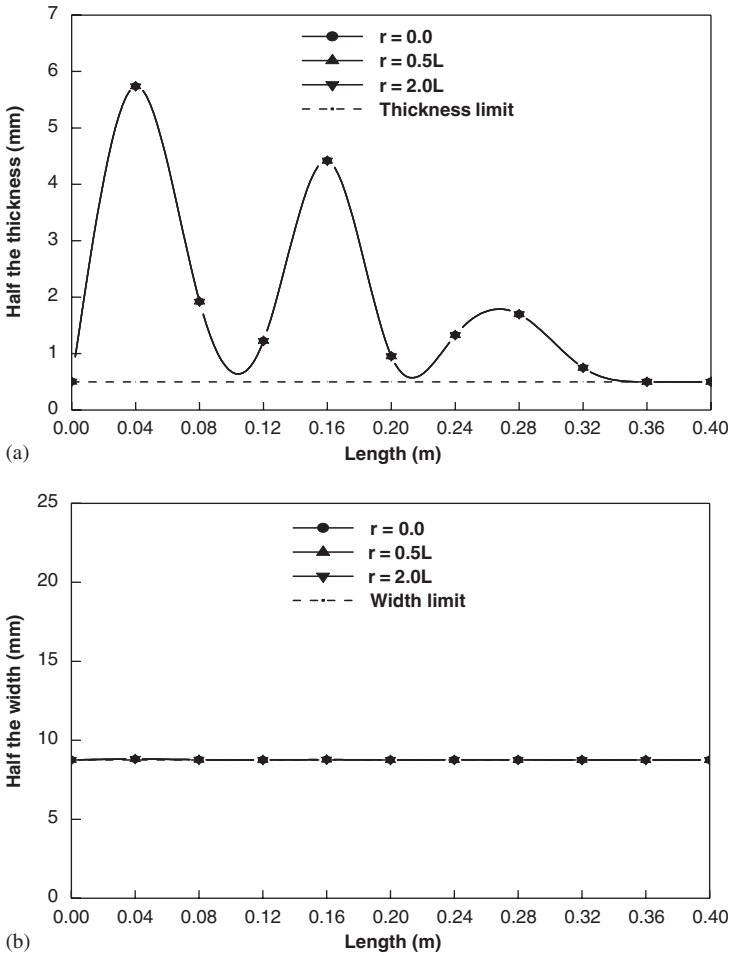

Fig. 9. Variation of the thickness and the width along the beam length that maximize the first natural frequency for three cases of hub radius. (a) Half the thickness, (b) half the width.

Fig. 10 shows the minimum and the maximum first natural frequency loci of the rotating beam when the angular speed increases from 0 to 100 rad/s. Thus, the two loci embrace the possible region of the first natural frequency. As shown in the figure, the first natural frequency is constrained to a value when the angular speed is 0 rad/s.

Figs. 11 and 12 show the thickness and the width of the beam versus the length of the beam for the minimum and the maximum first natural frequency results. The thickness and the width variations along the beam length with the angular speed of 100 rad/s are shown in these figures. Figs. 13 and 14 show the overall pictures of the beams for the minimum and the maximum frequency results, respectively. The thickness and the width are again amplified two times compared to the beam length.

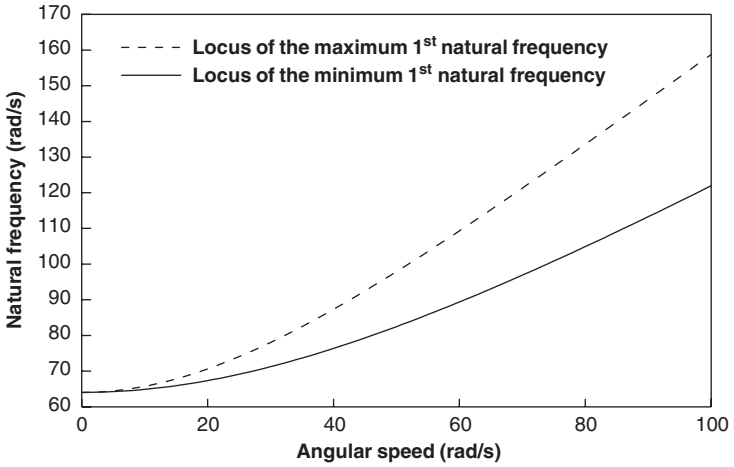

Fig. 10. The first natural frequency range for the optimization problem including the first natural frequency constraint at zero angular speed.

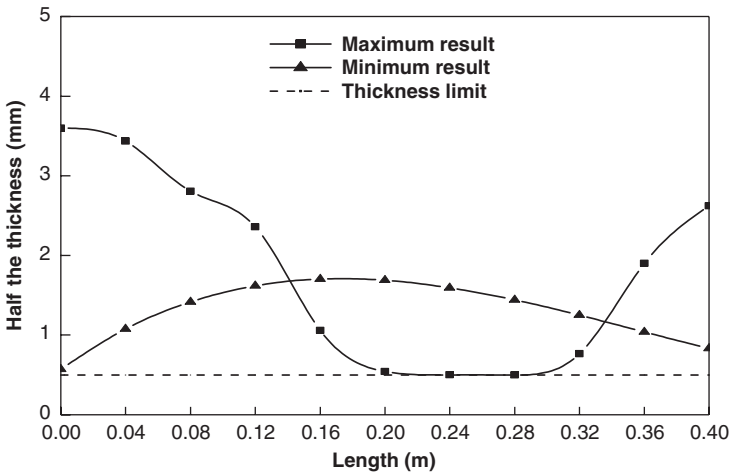

Fig. 11. Thickness variations that minimize and maximize the first natural frequency (for the optimization problems with an added constraint).

3.3. Problem to find a beam shape having a specified first natural frequency at a specific angular speed with the fixed stationary first natural frequency constraint

As a typical design problem, the first natural frequency of a rotating beam at a specific angular speed (usually this is the operating speed) is first determined to avoid undesirable problems like resonance phenomena. Then the beam shape that satisfies the condition needs to be found. To

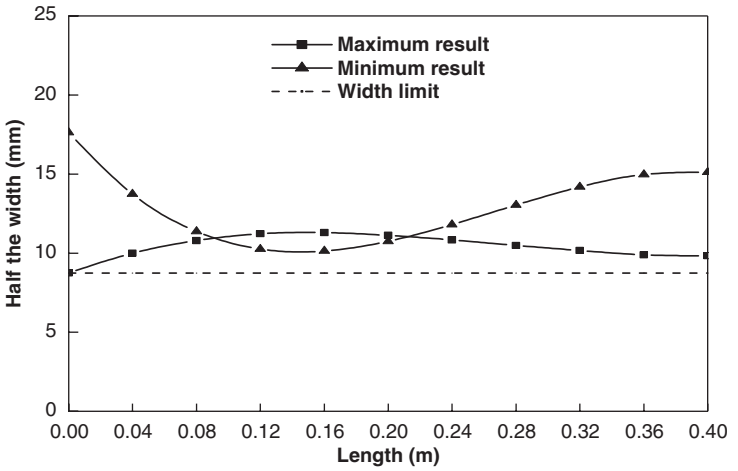

Fig. 12. Width variations that minimize and maximize the first natural frequency (for the optimization problems with an added constraint).

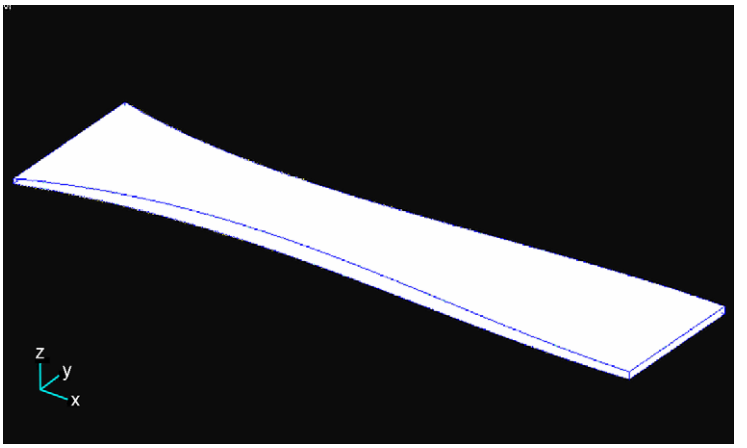

Fig. 13. Beam shape that minimizes the first natural frequency while satisfying the added constraint of the first natural frequency at zero angular speed.

solve such a design problem, the following formulation can be employed:

$$\begin{aligned} \text{Min} \quad & [\omega_1(\Omega_G, X) - \omega_G]^2 \\ \text{s.t.} \quad & \omega_1(0, X) - \omega_1(0, X_0) = 0, \\ & \int_0^L h(X,x)b(X,x)\,\mathrm{d}x \leqslant L h_{\text{ini}} b_{\text{ini}}, \\ & h(X,x) \geqslant h_{\min} \quad (0 \leqslant x \leqslant L), \\ & b(X,x) \geqslant b_{\min} \quad (0 \leqslant x \leqslant L), \end{aligned} \tag{26}$$

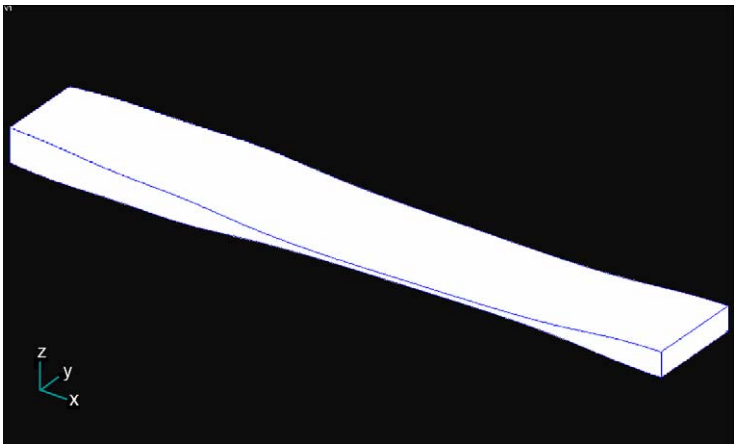

Fig. 14. Beam shape that maximizes the first natural frequency while satisfying the added constraint of the first natural frequency at zero angular speed.

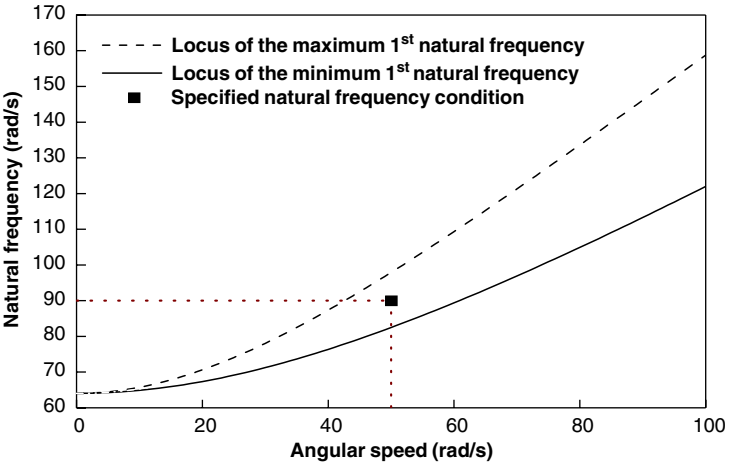

Fig. 15. A specified natural frequency condition at a non-zero angular speed that is located between the maximum and the minimum natural frequency loci.

where Ω_G and ω_G are the specific angular speed and the corresponding first natural frequency. The objective function is different from the previous problem but the constraint equations are same as the previous one.

Fig. 15 shows two loci and a point: the maximum first natural frequency locus, the minimum first natural frequency locus, and the point that satisfies $\omega_1(\Omega_G, X) - \omega_G = 0$. For this problem, Ω_G is given as 50 rad/s and ω_G is given as 90 rad/s. Of course, only the natural frequency that is located between the minimum and the maximum frequency loci may be required for the design problem. Fig. 16 shows the variations of the thickness and the width of the beam that has the specific natural frequency at the specific angular speed and Fig. 17 shows the overall picture of the

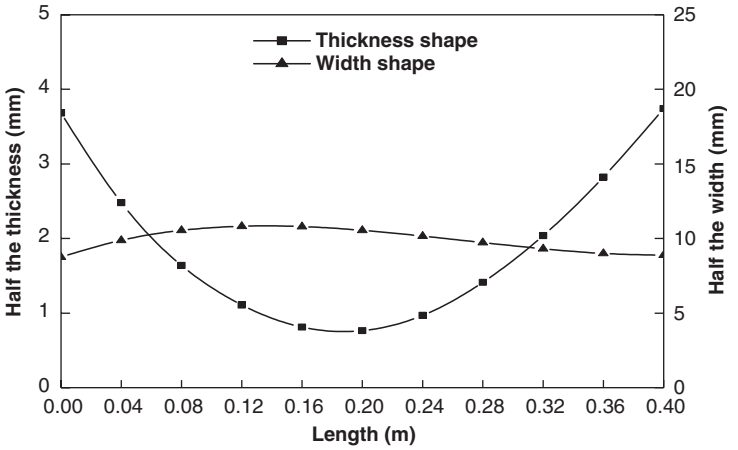

Fig. 16. Variations of the thickness and the width that satisfies a specified modal characteristic at a non-zero angular speed.

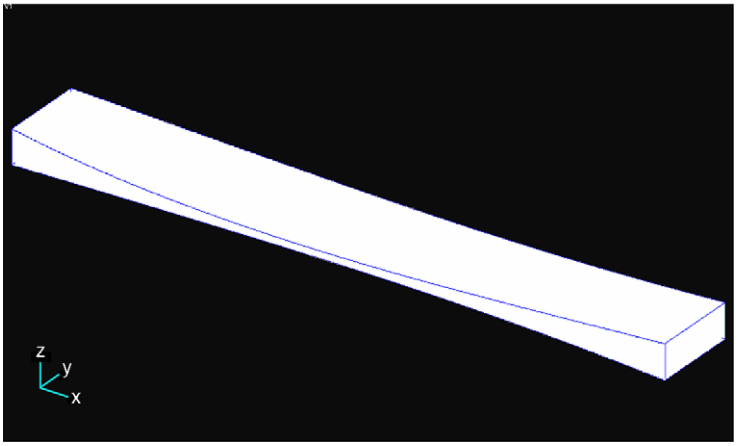

Fig. 17. Beam shape that satisfies a specified modal characteristic at a non-zero angular speed.

beam. The thickness and the width of the beam cross-section is again amplified two times compared to the length of the beam.

4. Conclusions

In this study, an optimization method is employed to find the cross-section shape variations of rotating cantilever beams that satisfy some specific modal characteristics. The beam is divided into multiple segments and the thickness and the width are assumed as cubic spline functions at the segments. The stage values of the thickness and the width are employed as design variables and

optimization problems to find the design variables are formulated. Numerical results show that there exist specific cross-section shape variations that satisfy certain modal characteristic requirements. It is also found that the angular speed and the hub radius little influence the optimal shapes of the rotating beams.

Acknowledgements

This research was supported by the Innovative Design Optimization Technology Engineering Research Center through the research fund, for which the authors are grateful.

References

[1] R. Southwell, F. Gough, The free transverse vibration of airscrew blades, British A.R.C. Reports and Memoranda, No. 766, 1921.
[2] R. Yntema, Simplified procedures and charts for the rapid estimation of bending frequencies of rotating beams, NACA 3459, 1955.
[3] M. Schilhansl, Bending frequency of a rotating cantilever beam, *Journal of Applied Mechanics* 25 (1958) 28–30.
[4] W. Carnegie, Vibrations of rotating cantilever blading: theoretical approaches to the frequency problem based on energy methods, *Journal of Mechanical Engineering Science* 1 (1959) 235–240.
[5] S. Putter, H. Manor, Natural frequencies of radial rotating beams, *Journal of Sound and Vibration* 56 (1978) 175–185.
[6] A. Wright, C. Smith, R. Thresher, J. Wang, Vibration modes of centrifugally stiffened beams, *Journal of Applied Mechanics* 49 (1982) 197–202.
[7] T. Kane, R. Ryan, A. Banerjee, Dynamics of cantilever beam attached to a moving base, *Journal of Guidance, Control, and Dynamics* 10 (1987) 139–151.
[8] K. Subrahmanyam, K. Kaza, G. Brown, C. Lawrence, Non-linear vibration and stability of rotating pre-twisted, preconed blades including Coriolis effects, *Journal of Aircraft* 24 (1987) 342–352.
[9] T. Yokoyama, Free vibration characteristics of rotating Timoshenko beams, *International Journal of Mechanical Sciences* 30 (1988) 743–755.
[10] Y. Kuo, T. Wu, S. Lee, Bending vibration of a rotating non-uniform beam with tip mass and an elastically restrained root, *Computers and Structures* 42 (1994) 229–236.
[11] H. Yoo, R. Ryan, R. Scott, Dynamics of flexible beams undergoing overall motions, *Journal of Sound and Vibration* 181 (1995) 261–278.
[12] H. Yoo, S. Shin, Vibration analysis of rotating cantilever beams, *Journal of Sound and Vibration* 212 (1998) 807–828.
[13] D. Goldberg, *Genetic Algorithms in Search, Optimization and Machine Learning*, Addison-Wesley, Longman, Reading, MA, 1989.
[14] G. Vanderplaats, DOT—Design Optimization Tools User Manual, Vanderplaats Research & Development, 1999.